Bound states of charges on top of graphene in a magnetic field

Sergey Slizovskiy*

Department of Physics, Loughborough University, Loughborough LE11 3TU, United Kingdom and NRC "Kurchatov Institute" PNPI, Russia

(Received 28 May 2015; revised manuscript received 22 September 2015; published 23 November 2015)

We show theoretically that in an external magnetic field, like charges on top of graphene monolayer may be mutually attracted to form macromolecules. For this to happen, graphene needs to be in a quantum Hall plateau state with the local chemical potential being between the Landau levels. One or several graphene electron(s) get localized in the middle between charges and provide overscreening of the Coulomb repulsion between the charges. The size of the resulting macromolecules is of the order of the magnetic length (∼10 nm for magnetic field 10 T). The possible stable macromolecules that unit charges can form on graphene in a magnetic field are classified. The binding survives significant temperatures, exceeding the mobility barriers for many ionically bond impurities. The influence of possible lattice-scale effects of valley mixing are discussed. Tuning the doping of graphene or the magnetic field, the binding of impurities can be turned on and off and the macromolecule size may be tuned. This opens the perspective to nanoscopic manipulation of ions on graphene by using magnetic field and gating.

DOI: 10.1103/PhysRevB.92.195426 PACS number(s): 75.70.Ak, 73.22.Pr, 12.20.Ds

I. INTRODUCTION

More than ten years since the discovery of graphene [1], the first genuinely two-dimensional material, are marked with a huge body of research. Its applications range from cancer-drug delivery [2,3] to novel electronic devices. Still, many of the proposed uses of graphene depend crucially on its interface interactions with other compounds and impurities. Typically, molecular dynamics and DFT methods [4–9] are used to model the interaction of graphene with substrate and impurities. It was shown that there are two types of impurity bonding to graphene [4]: covalently bond impurities (e.g., H, CH_3, F, OH, and O) and ionically bond impurities (e.g., Na, K, Cs, Cl, Br, and I). Covalently bond impurities act similar to the defects in graphene structure and typically have large mobility barriers, while ionically bond impurities have low mobility barriers (typically lower than room temperature) and act as mobile electric charges put on top of graphene [4,10,11].

The interaction between impurities has attracted significant experimental and theoretical interest. It was shown [12] that short-range covalently bond impurities tend to form bound clusters due to a fermionic Casimir effect with a binding energy comparable to the room temperature scale at distances below 2 nm. Related results were presented in Ref. [13] where dilute adatoms were shown to have a tendency towards a spatially correlated state with a hidden Kekulè mosaic order. On the other hand, this effect cannot compete with the Coulomb repulsion of like charges if the impurities are charged, as is the case for ionically bond impurities.

Graphene is known to be exceptionally susceptible to magnetic fields, with a divergent diamagnetic susceptibility at the Dirac point and strong nonlinear effects in the magnetization [14,15]. A magnetic field creates large energy gaps near the Dirac point that reduce intrinsic screening and help to localize electrons in the external potentials.

Without magnetic field, graphene will produce nonlinear screening of external charges [16,17]. When a magnetic field is applied, the ordinary screening is significantly suppressed [18,19] and electrons become localized.

In this work, we discuss the interaction between charged impurities near the surface of graphene in a strong magnetic field and show that in some cases the binding due to electrons in graphene can compete with Coulomb repulsion and stable nanomolecules may form. The motivation for this work comes not only from the ionically bond impurities mentioned above: epitaxial graphene on Si-terminated SiC [20–23] has an important feature of positively charged donors appearing dynamically in the "dead" carbon layer just below graphene [24–26]. This happens due to the dominant effect of quantum capacitance [27] and due to strong changes in the density of states near the Dirac point under the influence of a magnetic field [24,28]. The process looks as the appearance of localized holes in the insulating "dead" layer due to electrons transferred to graphene. Consequently, the charge transfer might dynamically create extra localized states and extra electrons to keep the system in a robust $\nu \approx 2$ quantum Hall plateau state. Since the charge transfer is reversible, the holes below graphene can be considered on the same footing as dynamical charged impurities. The process of charge transfer allows us to talk about a well-defined local value of the electron chemical potential. The chemical potential is chosen to be in the gap between the undisturbed Landau levels.

Another possible context is to consider the well-known semiclassical picture of the quantum Hall effect [29,30] (QHE). In this context, one typically assumes smooth (on the scale of the magnetic length) external potentials and derives the presence of compressible regions where electrons screen everything and incompressible regions that have exactly integer local filling factors. For nonsmooth potentials created by impurities close to graphene sheet, the semiclassical approach is not fully true. The self-consistent semiclassical approach gives a smoothly varying effective potential that could be locally treated as a chemical potential for our purpose. Our results imply that there is still some life in the incompressible region due to screening and possible overscreening of point charges, and thus the local filling factor of incompressible regions could deviate from integer values. Redistribution of mobile charges (holes in the substrate surface) can completely eliminate the compressible regions thus greatly increasing the precision of quantum Hall quantization.

*S.Slizovskiy@lboro.ac.uk

TABLE I. Phase diagram for N positively charged ions bound by n electrons at $\alpha = 0.4$ and $d = 0.05 l_B$; for negatively-charged ions, one has to replace $\mu \to -\mu$. $\mu_{\min}$ gives the minimal chemical potential for the existence of a given phase. Chemical potentials should be understood as taken relative to Landau level band edges, which are here renormalized to free-particle values 0 and $\sqrt{2}$ for easy match with free-particle levels. r_{ij} is the optimal distance between ions, i.e., the size of the molecule, measured in units of the magnetic length l_B. E is the minimal possible (binding) energy per molecule, which is achieved when μ tends to the band edge ($\mu = 0$ for configurations 1,...,5 and $\mu = \sqrt{2}$ for configurations 6,...,10). For lower μ, the energy to consider is $E - n\Delta\mu$. The last column, μ interval, indicates the range of chemical potentials where the phase gives the minimal energy per charge [see Eq.(10)].

No.	$\mu_{\min}$	N ions	n electrons	r_{ij}	E	μ interval
1	−0.93	3 △	2 symm.	1.5	−1.06	[−0.93, −0.75]
						[−0.55, −0.38]
2	−0.75	2	1	1.7	−0.52	[−0.75, −0.55]
3	−0.63	2	2 symm.	1.3	−0.96	[−0.38 , −0.08]
4	−0.45	1	1	–	−0.45	Ø
5	−0.28	1	2 symm.	–	−0.56	[−0.08,0]
6	0.51	3 △	2 symm.	1.4	−0.95	[0.51,0.67]
						[0.95,1.09]
7	0.67	2	1	1.5	−0.47	[0.67,0.95]
8	0.82	2	2 symm.	1.2	−0.85	[1.09,1.39]
9	1.02	1	1	–	−0.39	Ø
10	1.19	1	2 anti-s.	–	−0.45	[1.39,1.41]

For definiteness, we consider the positively charged ions below, but exactly the same description applies to the negative ions if one makes a particle-hole transformation and reverts the sign of chemical potential. We show that when several charged impurities are at a distance of the order of the magnetic length $l_B = \sqrt{\hbar/(eB)}$, they can form stable molecules bound by the electrons in graphene. Depending on its local chemical potential (taken in the region of a quantum Hall plateau), graphene may bind either positive ions, or negative, or produce no significant binding at all, the results are summarized in Table I and Fig. 4. The described effect may be called either as *overscreening of the Coulomb repulsion of impurities* or as *long-range covalent bonding of charged impurities*. A related "overscreening" effect exists for the charging of a quantum dot [31]; in colloidal systems, a similar effect is called "charge inversion" [32].

Graphene in a magnetic field hosts an electron hybridization cloud that can lead to an attraction exceeding the Coulomb repulsion of same-charge ions, see Fig. 1. Significant binding of charges occurs only when the electron cloud is centered

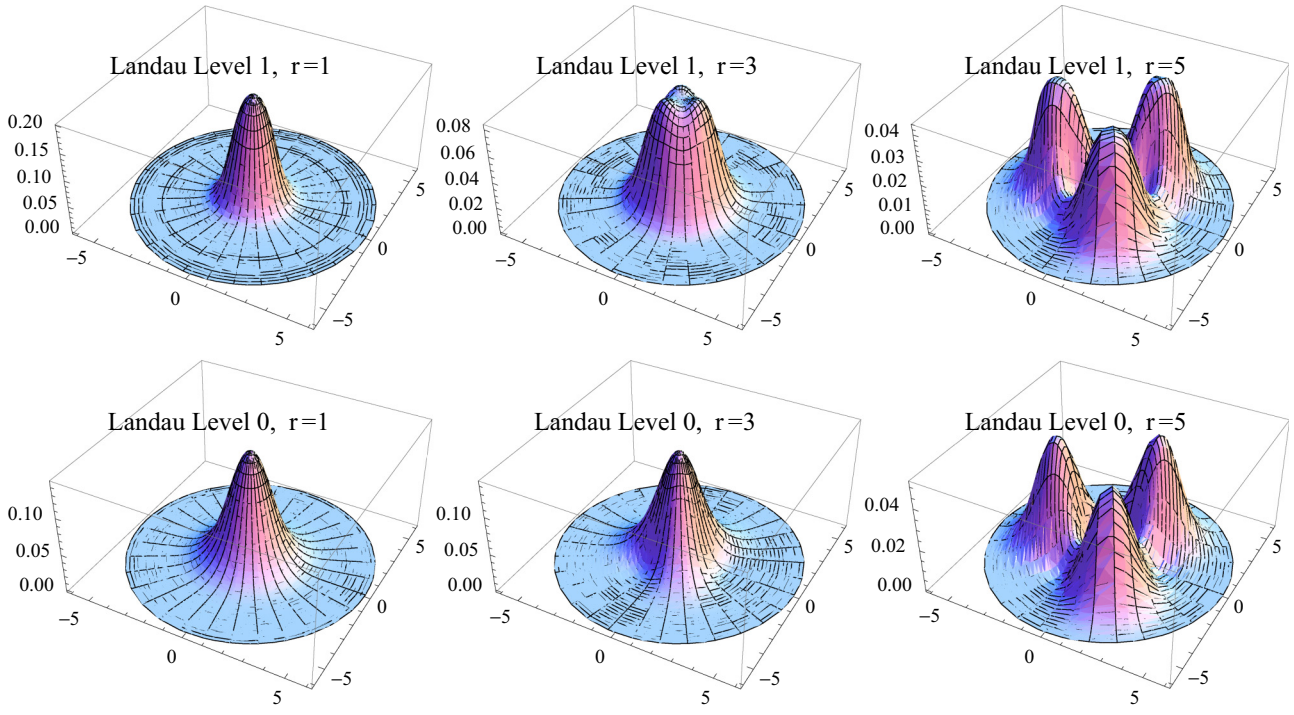

FIG. 1. (Color online) Electron densities for the *lowest sublevels* of the zeroth and first Landau levels in the field of three ions forming an equilateral triangle with sides r. Essential binding occurs for $r \lesssim 3 l_B$ where the electron wave function forms a single lump in the center.

in between the charges ($r \lesssim 3$ on Fig. 1). Similarly to the signatures of the QHE [33], we show that the effect may survive the room temperature for magnetic fields of order 10 T.

The paper has the following structure. In Sec. II, we introduce the formalism and present the results for bound states bound with one electron; in Sec. III, the results are generalized to multielectron bound states; in Sec. IV, the obtained results are combined in a phase diagram; in Sec. V, the qualitative effects of potentials that are nonsmooth on the lattice scale are discussed; conclusions are given in Sec. VI.

II. GRAPHENE WITH CHARGED IMPURITIES IN MAGNETIC FIELD

It is well-known that the one-particle energy levels of an ideal graphene in a magnetic field B are given by degenerate Landau levels [1,34–36]:

$$E_n = \mathrm{sign}(n) E_B \sqrt{2|n|}\ ,\ n \in \mathbb{Z}, \tag{1}$$

where $v_F \approx 10^6$ m/s,

$$l_B = \sqrt{\hbar/(eB)} \approx 26/\sqrt{B/(\mathrm{Tesla})}\ \mathrm{nm}, \tag{2}$$

$$E_B \equiv \frac{\hbar v_F}{l_B} \approx 26\sqrt{B/(\mathrm{Tesla})}\ \mathrm{meV}. \tag{3}$$

Each Landau level (LL) is degenerate with density $4\frac{e}{2\pi\hbar}B$ per unit area. Working with a finite area, it is convenient to use the basis of Landau wave functions in polar coordinates. Defining an oscillator radial eigenfunction

$$g_{n,m}(r) = e^{-\frac{r^2}{4}} r^{|m|} \sqrt{\frac{2^{-|m|}(|m|+n)!}{2\pi n!(|m|!)^2}}\ {}_1F_1\Big(-n; |m|+1; \frac{r^2}{2}\Big),$$

we have for the wave functions ($m < n$, $n > 0$):

$$\psi_{0,m}(r,\phi) = \begin{pmatrix} 0 \\ e^{im\phi} g_{0,m}(r) \end{pmatrix}, m \leqslant 0, \tag{4}$$

$$\psi_{\pm n,m}(r,\phi) = \frac{e^{im\phi}}{\sqrt{2}} \begin{pmatrix} \mp e^{-i\phi} g_{n-\frac{m-1+|m-1|}{2},m-1}(r) \\ i g_{n-\frac{m+|m|}{2},m}(r) \end{pmatrix}.$$

The solutions near the second K point are obtained by acting with $i\sigma_2$ on the spinor: $\binom{\Psi_1}{\Psi_2} \to \binom{\Psi_2}{-\Psi_1}$.

When the Coulomb impurity potential is present, the orbital (index m) degeneracy of Landau levels is lifted [19]. This has been calculated [19,37,38] and demonstrated experimentally [19] for one Coulomb impurity. Below we consider several impurities.

Consider a superposition of Coulomb potentials of the form

$$U(\vec{r}) = -\frac{e^2}{4\pi\epsilon_0\epsilon} \sum_i \frac{1}{\sqrt{(\vec{r}-\vec{r}_i)^2 + d^2}}. \tag{5}$$

Here the parameter d is a vertical displacement of impurity from the graphene sheet, but it can also be used to model a finite localization length of impurity wave function.[1] Here, there are two physical cases that may be considered. (1) The wave function of the localized impurity exceeds the graphene lattice scale, $d \gg a$, but still $d \ll l_B$. This will be the main topic of the present work. This may be relevant to the case when the localization of an impurity is determined by a Moire pattern formed by an incommensurate substrate and graphene. For epitaxial graphene on Si-terminated SiC this scale is estimated as $d \sim 2$ nm. Then the impurity potential is smooth on the lattice scale (note that it is still sharp on the scale of magnetic length) and single-valley continuum approximation works well, we may neglect the intervalley scattering. This means that the valley-mixing splitting is less than the interaction-induced energy and multielectron wave functions are determined by the long-range Coulomb interactions. This case is the most universal since it depends only on the magnetic length scale and the effective coupling constant. Additional universality comes from the fact that the dependence of the binding force on the effective range d of the impurity wave function is weak, see Fig. 5. (2) If the impurity is more like a point charge, then the impurity potential is sharp and nonuniversal lattice-scale details come into play and cause the valley mixing. Continuous approximation (7) breaks down near the impurity center since sharp potentials cause intervalley scattering. This is discussed in Sec. V. We discuss several lattice-related effects, but the main conclusions of the continuum-model considerations still hold true.

The equations for single-electron energy levels in graphene in the magnetic field B and any Coulomb potentials can be rewritten [37] in units of the magnetic length l_B, the magnetic energy E_B, and the dimensionless coupling

$$\alpha = e^2/(4\pi\epsilon_0\hbar v_F \epsilon_{\mathrm{eff}}) = 2.19/\epsilon_{\mathrm{eff}} \tag{6}$$

with the effective dielectric constant $\epsilon_{\mathrm{eff}} = (\epsilon_1 + \epsilon_2)/2$ coming from substrates on both sides of graphene and from graphene by itself. For example, $\alpha \approx 1$ on SiO_2 substrate [19] and $\alpha \approx 0.4$ on SiC. In dimensionless units, the equation to solve is [37]

$$[\sigma_1(i\partial_x - y) - i\sigma_2\partial_y]\Psi = \left(E - \sum_{i=1}^{N} \frac{\alpha}{\sqrt{(\vec{r}-\vec{r}_i)^2 + d^2}}\right)\Psi. \tag{7}$$

For "molecules" bound by more than one electron, we will account for e-e interactions below. To perform the computations, we evaluate the matrix elements of the impurity potential in the basis (4) truncated to several Landau levels (of the order of 10) and orbital states (of order of 30) and then do an exact diagonalization. In the case of smooth potentials, it is sufficient to consider only one valley. The truncation of orbital states we use corresponds to a circular box truncation of space, and to avoid unphysical boundary contributions, we had to smoothly cut off the Coulomb potential at large distances (of order of $4l_B$). As a result, for interior distances up to $2l_B$, the precision is better than 1%, while for larger distances the error may get higher.

The Landau levels that are completely filled do not contribute significantly to the energy of ions as a function of their separation (but they do contribute to the renormalization of the chemical potential [39,40]). This has been verified numerically and is seen analytically in the leading order of

[1] This way we may consider a hole in the "dead layer" of SiC epitaxial graphene as a mobile impurity.

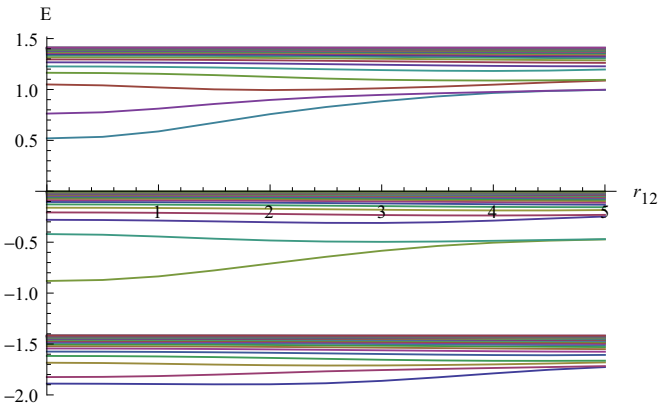

FIG. 2. (Color online) Plot of one-particle energy sublevels for several Landau levels as a function of the distance between two positively charged Coulomb centers. Here, $\alpha = 0.4$ and $d = 0.05$. A remarkable (but obvious) fact is that if all of the sublevels are populated, the distance dependence of the total energy disappears.

the perturbation theory in the potential:

$$E(r_{12}) \sim \sum_m \left\langle \psi^{(0)}_{n,m} \middle| V(\vec{r} - \vec{r}_1) + V(\vec{r} - \vec{r}_2) \middle| \psi^{(0)}_{n,m} \right\rangle$$
$$= 2 \sum_m \left\langle \psi^{(0)}_{n,m} \middle| V(\vec{r}) \middle| \psi^{(0)}_{n,m} \right\rangle = \text{const}, \quad (8)$$

where we used that the full degenerate set of wave functions, corresponding to a given Landau level (enumerated by m) maps to itself under translations (up to a unitary transformation), and so the above sum is independent of the impurity positions.

The situation changes drastically if only one or several lowest Landau sublevels are filled with electrons. This happens when graphene is in the quantum Hall plateau state corresponding to the chemical potential being in the gap below the band edge (i.e., between the unperturbed LLs in the one-particle picture).

Let us start with two positive charges $N = 2$. The single-particle energy levels of electrons in graphene are presented in Fig. 2. Note that only the lowest sublevels are fully meaningful as filling more levels requires to account for the e-e interactions.

When the distance between the two ions is of the order of the magnetic length l_B, the lowest energy electron wave function is *centered in the middle between the ions* and plays the role of a hybridization cloud that binds them, Fig. 1. When only this lowest-energy state is filled, a strong dependence of the energy on the distance r_{12} between ions appears, Fig. 2, creating an attractive force, Fig. 5. If the distance between charges exceeds roughly $3l_B$, the lowest energy electron wave function becomes centered near each of the individual charges and its energy depends on r_{12} as $E \sim -1/r_{12}$.

In the leading order of perturbation theory, the binding force is proportional to α. Notably, the mutual Coulomb repulsion of ions is also proportional to α:

$$E_{\text{Coulomb}} = \frac{\alpha}{r_{12}}. \quad (9)$$

Thus, in the leading approximation, the distance where the attraction would balance the repulsion is independent of α. We stress here that when expressed in magnetic length and energy units, there are essentially no free parameters in the problem and the Coulomb repulsion of ions is of the same order of magnitude as the hybridization attraction.[2] It is *a priori* not at all clear if stable bound states of ions can form. Moreover, strong bound states form only when the chemical potential μ is near the zeroth and first Landau levels. When μ is near the other Landau levels (see Fig. 2), the r_{12} dependence of the electron energy is substantially weaker leading to a weaker binding of ions. The main problem with bound states in the higher plateau states is that they will not survive graphene rippling and temperature, thus we concentrate on the most robust $\nu \approx \pm 2$ plateau states below.

Let us first study the dependence on the coupling constant α, see Fig. 5(b). We observe that the zeroth LL is almost protected from nonlinearity, while a significant nonlinearity appears in the higher LL already at $\alpha \sim 0.1$. The Landau levels 1 and -1 must have the same energies in the leading order of perturbation theory as their wave functions differ only by the relative sign of the sublattice components, but we see that these levels split already from $\alpha \sim 0.1$. This could be expected due to the large Coulomb field near an individual impurity. A similar asymmetry is present in the results of Ref. [19]. The dependence on the distance d of the ion from graphene (or, on the localization length of charge wave function) is weak when this distance is much less than the magnetic length, seexbrk Fig. 5(c).

Below, we present a particular example of $\alpha = 0.4$ and $d = 0.05 l_B$, the results are universal for zeroth LL, while for the first LL the binding is seen to grow a bit faster than linear in α.

The results for two positive ions bound by one electron are presented in Fig. 3(a). We observe an absolute minimum in the energy at a distance $r_{12\text{min}} \approx 1.5 l_B$ near the first LL or $1.7 l_B$ near the zeroth LL. If the chemical potential decreases below a critical value, determined as the energy per electron in the bound state, see Table I, there will be no bound states for positive ions, but, at some point, we start getting bound states for negatively charged impurities bound by holes. The calculations and results for negatively charged impurities are exactly the same and obtained by going to the hole picture.

An analogous calculation shows that the configurations with three symmetrically positioned impurities bound by one electron is unstable: despite an appearance of local energy minimum, the configuration would gain energy if deformed to a bound pair with the third ion repelled to infinity.

III. MULTIELECTRON STATES

Now consider multielectron bound states. The two-electron bound state can be in a symmetric or antisymmetric orbital state. In a conventional molecule, this would correspond to a spin singlet and a triplet, respectively, but in graphene, one has an additional valley degeneracy [14,41] and the full SU(4) symmetry is approximately respected (neglecting the

[2]This will not be the case for the ordinary 2D electron gas since the quasiparticle mass will essentially enter the game.

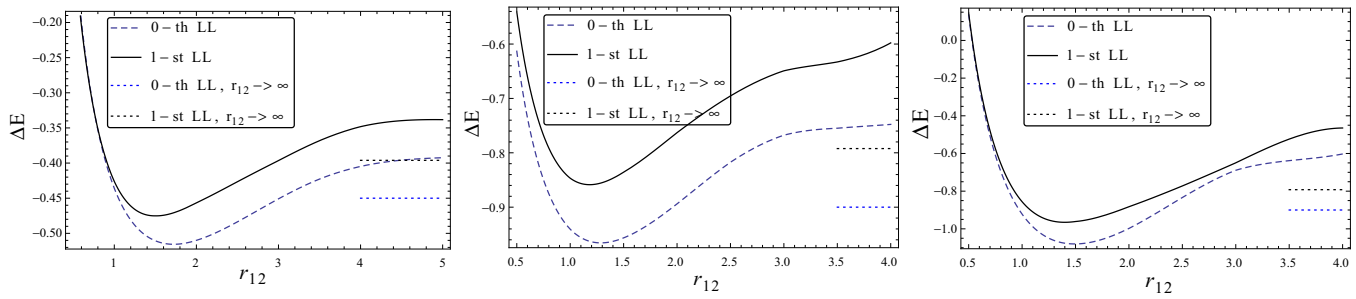

FIG. 3. (Color online) Energy (electron energy + Coulomb repulsion of ions) of stable macromolecules. The electron energy is counted from the Landau level edge (fixed to free-particle values 0 and $\sqrt{2}$ for zeroth and first LLs respectively). Here, $\alpha = 0.4$ and $d = 0.05l_B$. Dotted lines mark the $r \to \infty$ asymptotic to show stability. (a) Two ions bound by one electron in graphene. (b) Two ions bound by two electrons in a symmetric orbital state. (c) Three ions forming an equilateral triangle bound by two electrons in a symmetric state.

Zeeman splitting and valley mixing). Group theory tells us that $\mathbf{4} \otimes \mathbf{4} = \mathbf{10} \oplus \mathbf{6}$ in spin-valley space, so, there are ten possibilities to form an antisymmetric orbital state and six for a symmetric one. If the valley-mixing effects discussed in Sec. V are important (exceed the temperature scale), then the orbital-symmetric state will be the usual spin singlet.

To find a reasonable approximation to the energy, we use the variational Hartree-Fock method with a basis formed by the Slater determinants of low-energy one-particle eigenstates found above. Looking at Fig. 2, we note that near the first LL, the two lowest single-particle energy sublevels grow with r_{12} thus can potentially bind the ions and can participate in an antisymmetric orbital wave function. For the zeroth LL, only the lowest sublevel binds the ions while electrons in the higher levels do not tend to hybridize, thus the orbital wave function should be symmetric for a stable ion binding. These conclusions were checked by explicit computations and comparison of the energy.

Consider two electrons in the field of a single ion. For $\alpha = 0.4$, we have energies -0.28 and -0.21 per electron in zeroth and first LL, respectively, for a symmetric state and -0.24, and -0.22, respectively, for an antisymmetric orbital. Thus we expect a symmetric state near zeroth LL and an antisymmetric state near the first LL. A calculation shows that one unit-charge ion cannot hold more than two electrons in the lowest-energy states: e-e interactions make this too expensive.

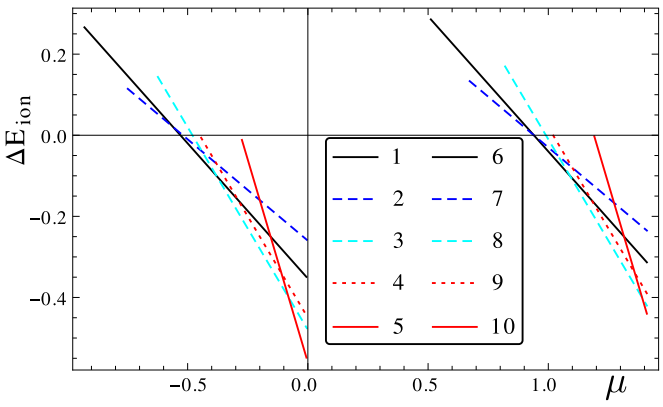

FIG. 4. (Color online) Zero-temperature phase energy plot for dilute mobile charged impurities. The phase with the lowest ΔE_{ion} is favored. The legend corresponds to Table I. The chemical potential should be understood as taken relative to the Landau level edges, which in this plot are renormalized to the free-particle values of 0 and $\sqrt{2}$.

Now we consider two positive charges and two electrons. A calculation shows that a symmetric orbital state is preferred. The resulting hydrogenlike molecule is very stable with an optimal interatomic distance of $1.2l_B$ and $1.3l_B$ for the first and zeroth LL, Fig. 3(b).

The same calculation can be repeated for three ions bound by two electrons, see Fig. 3(c). We compare the triangle configuration of ions with a linear chain geometry and find that the equilateral triangle geometry has lower energy. The described equilateral triangle with two electrons is prominent for providing the lowest possible energy per electron, thus, it is this configuration that appears first in the phase diagram, Table I. Four ions cannot be bound by two electrons.

Considering now three-electron states in the Hartree approximation, we found that three electrons cannot form a one-centered wave function to bind any number of ions since the e-e interaction gets too high and the resulting energy gain can by no means compete with the energy of far-separated smaller clusters described above. The situation is different from the ordinary molecules since the shape of the wave function is mostly determined by the Landau level number and not by the Coulomb potential of charges. For the lowest Landau levels that are most robust, the shape of wave functions is essentially circular (similar to s state). The above considerations still do not exclude the possibility of larger multielectron bound states with a *multicentered electron wave function*, but a quantitative study of such configurations is beyond the scope of this paper.

IV. PHASE DIAGRAM

Having studied the simple macromolecules separately, the results may be combined in a phase diagram, see Table I. In each of the above states, one can find the energy per electron that binds the molecule and thus find a minimal electron chemical potential $\mu_{\min}$ for such a molecule to appear. For a given electron chemical potential, several molecule configurations may be possible. Let us assume that the number of ions and the electron chemical potential are fixed. For a molecule with N ions bound by n electrons, we compute the free energy gain per ion by the formula

$$\Delta E_{\text{ion}} = \frac{(E_{\text{binding}} + E_{\text{Coulomb}}) - \mu n}{N} = \frac{E - \mu n}{N}. \quad (10)$$

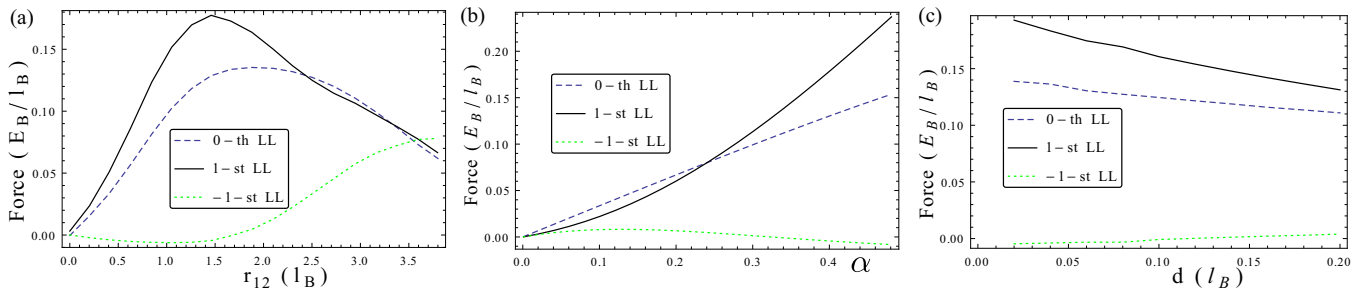

FIG. 5. (Color online) Binding force of two ions bound by one electron: (a) as a function of inter-ion distance r_{12} for $\alpha = 0.4$ and $d = 0.05l_B$; (b) as a function of coupling α for $d = 0.05l_B$ and $r_{12} = 1.5l_B$; and (c) as a function of d (distance of ions from the graphene sheet) for $\alpha = 0.4$, $r_{12} = 1.5l_B$

The configurations with minimal $\Delta E_{\rm ion}$ will deliver the minimal free energy at zero temperature, see Fig. 4. In particular, Fig. 4 shows that the state of one electron bound by one ion (lines 4 and 9 on the plot) is never the lowest-energy state. At high chemical potentials (close to the vacuum LL) the state with two electrons per one ion wins (lines 5 and 10). All the other states correspond to bound states of two or three ions, which are realized when $\mu \in [-0.93,-0.08] \cup [0.51,1.39]$ for the example $\alpha = 0.4$ considered. Note that for $\mu < -0.51$ and $\mu < 0.95$ the bound states are meta-stable since $\Delta E_{\rm ion}$ is positive. Finite density of charges may protect such states from decaying.

Changing α in the leading approximation just linearly scales the phase diagram around the vacuum Landau level (0 and $\sqrt{2}$). As is seen from Fig. 5, the binding of molecules near $\nu = 2$ should additionally increase with increasing α due to noticeable nonlinearity.

To come to physical conclusions, consider a realistic example of randomly positioned charges. For example, consider four charges and the $\nu \approx 2$ plateau state. Looking at the Table I, we can find the states that deliver the best binding energy per charge as follows. (1) If the chemical potential is $\mu \in [0.51,0.67]$, three charges may be bound with two electrons in the triangle (state 6) and the fourth is repelled to infinity since no electrons can be bound to it. In reality, it would be hard to create such a state since one needs to surpass a significant Coulomb repulsion gap to form the triatomic molecule. (2) If $\mu \in [0.67,1.02]$, two diatomic ions (two ions bound with one electron) would be the preferred state (again, it will be hard to create). The state 1 will continue to exist as well. (3) For $\mu > 1.02$, a single charge can bind an electron, forming a neutral combination. Now it is much easier to form molecules since there is no long-range Coulomb barrier. In particular, the triatomic configuration (No. 6 in the table) is now much easier to form, note that this configuration has unit total positive charge. One remaining charge will have one electron bound to it and this neutral combination will be attracted by the induced dipole moment to any charged object. Thus a four-atom molecule may be formed. The precise determination of its energy is beyond the scope of this paper. (4) For $\mu > 1.09$, the diatomic charged configurations (No. 6) would shrink in size (from 1.5 to 1.2) to form the neutral diatomic molecules (No. 8).

Analyzing the above example we may draw the following conclusions. If there are randomly positioned same-charge mobile impurities, the active recombination process would start only when neutral states of one impurity and one electron (No. 4 or No. 9) may be formed. For a lower chemical potential, stable bound states exist but they are hard to form due to significant Coulomb repulsion barriers. The most relevant recombination channel is to form a neutral hydrogenlike molecule (No. 3 or No. 8). In general, the clustering process is mediated by the induced dipole attraction of neutral and charged macromolecules.

If we are dealing not with real ionic impurities, but with holes dynamically appearing in the surface layer of a substrate below graphene, the Coulomb barriers for the formation of bound states are much lower and all the states in Table I are relevant. Their appearance will be governed by the *local* chemical potential formed by other nonmobile charges.

It should be kept in mind that all these calculations make sense when the concentration of the mobile impurities is low: $n_{\rm imp} \ll l_B^{-2}$. Correspondingly, the filling factor of electrons that bind these impurities must be very close to the perfect values ± 2. These conditions could easily be achieved *locally* in the incompressible regions appearing dynamically in the QHE physics. All the "extra" electrons are expelled out to compressible regions.

V. VALLEY MIXING AND LATTICE EFFECTS

In the case of sharp potentials, we need to consider the doubled basis, involving the Landau level states in both valleys. Naively, the matrix element between the Landau states could be computed by discrete lattice summation in the circle around the impurity and with continuum integration in the other regions. On the other hand, using only Coulomb interaction and Dirac bands in the immediate vicinity of the impurity would be an oversimplification and the full (e.g., DFT) study including a high-energy band is needed. Thus we follow a phenomenological approach and model the impurity as a smoothed Coulomb potential (as studied above) supplemented with pointlike scatterers sitting on A and (or) B sublattices. According to Ref. [4], positively charged impurities (Li, Na,K, Cs) tend to be located in the center of graphene hexagons ("h point") and the negative impurities (Cl,Br,I) prefer to stay on top of carbon atoms ("t point"). Thus it is natural to expect a sublattice-symmetric effective potential for positive ions ($V_{Ai} = V_{Bi}$) and a sublattice-asymmetric potential for negative impurities. In the latter case, similarly to Ref. [12],

it is interesting to study the difference of same-sublattice and different-sublattice locations of impurities. A general point potential is parameterized by its sublattice components $V_{AAi}, V_{BBi}, V_{ABi}$ at each of the impurity positions x_i. These components are naturally combined in a 2×2 matrix $V(x_i)$.

In the leading order of perturbation theory, these potentials shift and split the single-valley energy levels discussed above. Let us consider corrections to the energies of one-electron bound states in the field of N impurities. The wave functions with the same energy E_0 in the second valley are obtained as $\Psi_{K'} = i\sigma_2\Psi_K$. To discuss the lifting of this degeneracy in the leading order of perturbation theory, we have the Hamiltonian $H = \begin{pmatrix} E_0+V_{11}, & V_{12} \\ V_{12}^*, & E_0+V_{22} \end{pmatrix}$ with matrix elements

$$V_{11} = \sum_{j=1}^{N} \Psi^\dagger(x_j) V(x_j) \Psi(x_j), \tag{11}$$

$$V_{12} = \sum_{j=1}^{N} \Psi^\dagger(x_j) V(x_j) i\sigma_2 \Psi(x_j), \tag{12}$$

$$V_{22} = \sum_{j=1}^{N} \Psi^\dagger(x_j) \sigma_2 V(x_j) \sigma_2 \Psi(x_j). \tag{13}$$

The energy eigenvalues are

$$E = E_0 + \frac{V_{11}+V_{22}}{2} \pm \sqrt{\left(\frac{V_{11}-V_{22}}{2}\right)^2 + |V_{12}|^2}. \tag{14}$$

Note that the sublattice components of the wave functions for the zeroth and the first Landau levels are strongly asymmetric: one sublattice component is dominant for a chosen valley, see Fig. 6. Hence, with a good accuracy, valley matrix elements are proportional to sublattice matrix elements: $V_{11} \sim \sum_i V_{BBi}|\Psi(x_i)|^2$, $V_{22} \sim \sum_i V_{AAi}|\Psi(x_i)|^2$, and $V_{12} \sim \sum_i V_{ABi}|\Psi(x_i)|^2$. For negatively charged ions situated on the same sublattice, we get the main nonzero matrix element $V_{11} = 2V$. This shifts down the energy in one of the valleys by $2|V|$. If the impurities are on different sublattices, we get $V_{11} = V_{22} = V$, which gives an equal twice smaller energy shift $|V|$ for both valleys. Thus the location of impurities on the same sublattice is energetically preferred and the corresponding electronic wave function prefers this sublattice (assuming that $V < 0$).

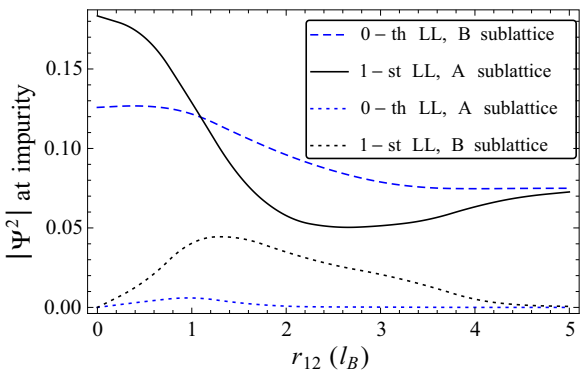

FIG. 6. (Color online) Plot of sublattice components of wave functions for lowest-energy sublevels of zeroth and first Landau Levels in the field of two charges at distance r_{12}. Wave functions are evaluated at the location of charged impurities.

For positively-charged ionic impurities, one expects $V_{11} = V_{22}$ due to preferred location of impurity in the centers of hexagons. Then the sublattice-mixing matrix element V_{12} plays the leading role in lifting the valley degeneracy. The preferable wave function would then be a symmetric or antisymmetric combination of both valleys or sublattices.

Both effects advocated above lead to an extra gain in binding energy that would depend on the distance between the impurities, thus, producing an extra force. The distance dependence is governed by $|\Psi(x_i)^2|$, which, as already stated, is dominated by only one sublattice component, see Fig. 6.

Figure 6 illustrates that the effects related to scattering on sharp potentials do further increase the binding force. The two-electron states discussed before essentially fill the same orbital state with two electrons, hence, the discussed correction just doubles. The matrix elements discussed above scale with the magnetic field as $|\psi^2(x_i)| \sim 1/l_B^2 \sim B$. The resulting extra contribution to energy scales as B and the force scales as $B^{3/2}$. This is to be compared with $B^{1/2}$ scaling of the main term in the energy.

VI. DISCUSSION AND CONCLUSIONS

To conclude, we have shown that for a significant range of chemical potential values inside the gap between Landau levels, the charged impurities (or donor states in the substrate surface) can form stable bound states. The optimal distance between charges in the bound state is of the order of the magnetic length $l_B = \sqrt{\hbar/(eB)}$. The binding energy scales as $E_B = \frac{\hbar v_F}{l_B}$ and the binding force at optimal distance scales as $F \sim E_B/l_B \sim v_F eB$.

The above results were obtained for an ideal monolayer graphene sheet at zero temperature. The realistic graphene may have other nonmobile impurities, ripples, corrugations, and finite temperature. Clearly, mobile charge impurities can equally well form bound states with the nonmobile ones. Simultaneously, charged impurities may introduce smooth inhomogeneities in the chemical potential leading to replacement of chemical potential μ with a local chemical potential $\mu + U_{\text{impurities}}$ in our considerations. It is also important to note that a sufficient amount of mobile charged impurities leads to screening of potential landscape thus making it flatter on large scales. This may be one of the keys to the understanding of exceptionally precise Hall quantization in epitaxial graphene [25].

The temperature and short-range impurities lead to level broadening. As is clear from Fig. 2, the binding appears when the lowest Landau sublevel is filled, while the next ones are empty. The splitting between these levels is of the order of $\alpha E_B \approx 300\alpha\sqrt{B/(\text{Tesla})}$ K (see Fig. 2). The splitting of levels is twice smaller near the first LL, but in this case, the second smallest LL is also attractive and the population of this level does not spoil the binding. So, with $\alpha \approx 0.4$, our results must survive the room temperatures and a small amount of short-range impurities for magnetic fields above 10 T and even higher temperatures at larger fields. These conclusions are also supported by the experiment of Ref. [19]. Note that

at room temperature (and even below) many types of ionic impurities are mobile [4].

Another effect of the finite temperature is an entropic contribution coming from the approximate spin and valley degeneracy. This effectively decreases the energy by $k_B T \ln n$, where $n = 4$ for one-electron bound states, $n = 6$ for two-electron symmetric states, and $n = 10$ for two-electron antisymmetric states. These numbers are to be changed if the degeneracy lifting due to the local lattice effects discussed in Sec. V or Zeeman splitting exceeds the temperature scale.

An important aspect in graphene is rippling and corrugations [42–44]. As argued in Ref. [45], corrugations in graphene may be described by fluctuations in a perpendicular magnetic field that lead to considerable broadening of nonzero LLs. At the same time, the zeroth LL is protected and mainly broadens due to temperature [45]. Our main results correspond to chemical potentials in the gap above or below the zeroth LL, thus the effect of corrugations is expected to be moderate. At the same time, corrugations may kill any weak binding effects that might occur in the higher QHE plateaux.

To summarize, we have shown that graphene in a magnetic field can mediate strong attraction of like charges put near graphene. The resulting size and configuration of macromolecules depend on the magnetic length and local chemical potential and thus can be easily changed by tuning the magnetic field or doping of graphene. The results are expected to survive significant temperatures. This opens a perspective to nanoscopic manipulation of ions on graphene by using macroscopic tools and provides further insight onto the structure of incompressible regions in QHE physics beyond the semiclassical approximation. Apart from that, the results might shed light on the microscopic structure of the potential landscape in SiC epitaxial quantum Hall effect devices.

ACKNOWLEDGMENTS

This work has been supported by EPSRC through Grants EP/l02669X/1 and EP/H049797/1. The support of the Russian Science Foundation Grant 14-22-00281 is acknowledged. I am indebted to Joseph J. Betouras and Feo V. Kusmartsev for many stimulating discussions and support. Useful correspondence with A.Tzalenchuk, O.Gamayun, and G.Berdiyorov is gratefully acknowledged. Important comments and suggestions of the referees are acknowledged.

[1] K. S. Novoselov, A. K. Geim, S. V. Morozov, D. Jiang, M. I. Katsnelson, I. V. Grigorieva, S. V. Dubonos, and A. A. Firsov, Nature (London) **438**, 197 (2005).
[2] M. Biggs, M. Kiamahalleh, M. Mijajlovic, and M. Penna, AU2014/900273 (2014).
[3] M. Biggs, M. Penna, M. Kiamahalleh, and M. Mijajlovic, PCT/AU2015/000034 (2015).
[4] T. O. Wehling, M. I. Katsnelson, and A. I. Lichtenstein, Phys. Rev. B **80**, 085428 (2009).
[5] K.-H. Jin, S.-M. Choi, and S.-H. Jhi, Phys. Rev. B **82**, 033414 (2010).
[6] M. Khantha, N. A. Cordero, L. M. Molina, J. A. Alonso, and L. A. Girifalco, Phys. Rev. B **70**, 125422 (2004).
[7] A. N. Rudenko, F. J. Keil, M. I. Katsnelson, and A. I. Lichtenstein, Phys. Rev. B **82**, 035427 (2010).
[8] P. V. C. Medeiros, A. J. S. Mascarenhas, F. de Brito Mota, and C. M. C. de Castilho, Nanotechnol. **21**, 485701 (2010).
[9] S. Y. Davydov and G. I. Sabirova, Tech. Phys. Lett. **37**, 515 (2011).
[10] F. Schedin, A. K. Geim, S. V. Morozov, E. W. Hill, P. Blake, M. I. Katsnelson, and K. S. Novoselov, Nat. Mater. **6**, 652 (2007).
[11] M. Caragiu and S. Finberg, J. Phys. Condens. Matter **17**, R995 (2005).
[12] A. V. Shytov, D. A. Abanin, and L. S. Levitov, Phys. Rev. Lett. **103**, 016806 (2009).
[13] V. Cheianov, V. Falko, O. Syljusen, and B. Altshuler, Solid State Commun. **149**, 1499 (2009).
[14] M. O. Goerbig, Rev. Mod. Phys. **83**, 1193 (2011).
[15] S. Slizovskiy and J. J. Betouras, Phys. Rev. B **86**, 125440 (2012).
[16] M. M. Fogler, D. S. Novikov, and B. I. Shklovskii, Phys. Rev. B **76**, 233402 (2007).
[17] I. S. Terekhov, A. I. Milstein, V. N. Kotov, and O. P. Sushkov, Phys. Rev. Lett. **100**, 076803 (2008).
[18] P. K. Pyatkovskiy and V. P. Gusynin, Phys. Rev. B **83**, 075422 (2011).
[19] A. Luican-Mayer, M. Kharitonov, G. Li, C.-P. Lu, I. Skachko, Alem-Mar B. Gonçalves, K. Watanabe, T. Taniguchi, and E. Y. Andrei, Phys. Rev. Lett. **112**, 036804 (2014).
[20] H. Tetlow, J. P. de Boer, I. J. Ford, D. D. Vvedensky, J. Coraux, and L. Kantorovich, Phys. Rep. **542**, 195 (2014).
[21] S. Kim, J. Ihm, H. J. Choi, and Y.-W. Son, Solid State Commun. **175**, 83 (2013).
[22] Y. Qi, S. H. Rhim, G. F. Sun, M. Weinert, and L. Li, Phys. Rev. Lett. **105**, 085502 (2010).
[23] F. Varchon, R. Feng, J. Hass, X. Li, B. N. Nguyen, C. Naud, P. Mallet, J.-Y. Veuillen, C. Berger, E. H. Conrad, and L. Magaud, Phys. Rev. Lett. **99**, 126805 (2007).
[24] T. J. B. M. Janssen, A. Tzalenchuk, R. Yakimova, S. Kubatkin, S. Lara-Avila, S. Kopylov, and V. I. Fal'ko, Phys. Rev. B **83**, 233402 (2011).
[25] A. Tzalenchuk, S. Lara-Avila, A. Kalaboukhov, S. Paolillo, M. Syväjärvi, R. Yakimova, O. Kazakova, T. J. B. M. Janssen, V. Fal'Ko, and S. Kubatkin, Nat. Nanotechnol. **5**, 186 (2010).
[26] J. A. Alexander-Webber, A. M. R. Baker, T. J. B. M. Janssen, A. Tzalenchuk, S. Lara-Avila, S. Kubatkin, R. Yakimova, B. A. Piot, D. K. Maude, and R. J. Nicholas, Phys. Rev. Lett. **111**, 096601 (2013).
[27] S. Kopylov, A. Tzalenchuk, S. Kubatkin, and V. I. Fal'ko, Appl. Phys. Lett. **97**, 112109 (2010).
[28] S. Slizovskiy, J. Phys. Condens. Matter **25**, 496007 (2013).
[29] D. B. Chklovskii, B. I. Shklovskii, and L. I. Glazman, Phys. Rev. B **46**, 4026 (1992).
[30] K. Lier and R. R. Gerhardts, Phys. Rev. B **50**, 7757 (1994).
[31] A. A. Koulakov and B. I. Shklovskii, Philos. Mag. B **77**, 1235 (1998).
[32] A. Y. Grosberg, T. T. Nguyen, and B. I. Shklovskii, Rev. Mod. Phys. **74**, 329 (2002).

[33] K. S. Novoselov, Z. Jiang, Y. Zhang, S. V. Morozov, H. L. Stormer, U. Zeitler, J. C. Maan, G. S. Boebinger, P. Kim, and A. K. Geim, Science **315**, 1379 (2007).
[34] Y. Zhang, Y.-W. Tan, H. L. Stormer, and P. Kim, Nature (London) **438**, 201 (2005).
[35] V. P. Gusynin and S. G. Sharapov, Phys. Rev. Lett. **95**, 146801 (2005).
[36] N. M. R. Peres, F. Guinea, and A. H. Castro Neto, Phys. Rev. B **73**, 125411 (2006).
[37] O. V. Gamayun, E. V. Gorbar, and V. P. Gusynin, Phys. Rev. B **83**, 235104 (2011).
[38] Y. Zhang, Y. Barlas, and K. Yang, Phys. Rev. B **85**, 165423 (2012).
[39] G. Fano and F. Ortolani, Phys. Rev. B **37**, 8179 (1988).
[40] B. Skinner and B. I. Shklovskii, Phys. Rev. B **87**, 035409 (2013).
[41] A. H. Castro Neto, F. Guinea, N. M. R. Peres, K. S. Novoselov, and A. K. Geim, Rev. Mod. Phys. **81**, 109 (2009).
[42] S. V. Morozov, K. S. Novoselov, M. I. Katsnelson, F. Schedin, L. A. Ponomarenko, D. Jiang, and A. K. Geim, Phys. Rev. Lett. **97**, 016801 (2006).
[43] J. C. Meyer, A. K. Geim, M. I. Katsnelson, K. S. Novoselov, T. J. Booth, and S. Roth, Nature (London) **446**, 60 (2007)
[44] M. I. Katsnelson and K. S. Novoselov, Solid State Commun. **143**, 3 (2007).
[45] A. J. M. Giesbers, U. Zeitler, M. I. Katsnelson, L. A. Ponomarenko, T. M. Mohiuddin, and J. C. Maan, Phys. Rev. Lett. **99**, 206803 (2007).